

RESEARCH LETTER

10.1002/2016GL072488

Key Points:

- Extreme waves will change along a large portion of the coasts generally increasing in the S. Hemisphere and decreasing in the N. Hemisphere
- The projected changes of extreme waves can be explained with a projected intensification of climatic patterns such as AAO, ENSO, and NAO

Supporting Information:

- Supporting Information S1

Correspondence to:

L. Mentaschi,
lorenzo.mentaschi@ec.europa.eu

Citation:

Mentaschi, L., M. I. Vousdoukas, E. Voukouvalas, A. Dosio, and L. Feyen (2017), Global changes of extreme coastal wave energy fluxes triggered by intensified teleconnection patterns, *Geophys. Res. Lett.*, *44*, 2416–2426, doi:10.1002/2016GL072488.

Received 31 DEC 2016



Accepted 31 JAN 2017

Published online 13 MAR 2017

©2017. The Authors.

This is an open access article under the terms of the Creative Commons Attribution-NonCommercial-NoDerivs License, which permits use and distribution in any medium, provided the original work is properly cited, the use is non-commercial and no modifications or adaptations are made.

Global changes of extreme coastal wave energy fluxes triggered by intensified teleconnection patterns

Lorenzo Mentaschi¹ , Michalis I. Vousdoukas^{1,2} , Evangelos Voukouvalas¹ , Alessandro Dosio¹ , and Luc Feyen¹
¹Joint Research Centre, European Commission, Ispra, Italy, ²Department of Marine Sciences, University of the Aegean, Mitilene, Greece

Abstract In this study we conducted a comprehensive modeling analysis to identify global trends in extreme wave energy flux (WEF) along coastlines in the 21st century under a high emission pathway (Representative Concentration Pathways 8.5). For the end of the century, results show a significant increase up to 30% in 100 year return level WEF for the majority of the coastal areas of the southern temperate zone, while in the Northern Hemisphere large coastal areas are characterized by a significant negative trend. We show that the most significant long-term trends of extreme WEF can be explained by intensification of teleconnection patterns such as the Antarctic Oscillation, El Niño–Southern Oscillation, and North Atlantic Oscillation. The projected changes will have broad implications for ocean engineering applications and disaster risk management. Especially low-lying coastal countries in the Southern Hemisphere will be particularly vulnerable due to the combined effects of projected relative sea level rise and more extreme wave activities.

1. Introduction

Waves are a prominent component of coastal hazard, contributing to extreme water levels manifested as wave setup and runup [Stockdon et al., 2006; Hemer et al., 2012; Vousdoukas et al., 2012a]. Extreme waves transfer large amounts of energy to the coast, applying huge stress to coastal installations and protection structures [Oumeraci, 1994; Van der Meer et al., 2016], accelerating sediment transport processes and coastal erosion [Masselink and Puleo, 2006; Vousdoukas et al., 2012b; Archetti et al., 2016; Masselink et al., 2016; Monioudi, 2016; Postacchini et al., 2017], and driving dune breaching [Matias et al., 2008; Roelvink et al., 2009] and inundation [Bertin et al., 2012; Vousdoukas et al., 2016b]. By modulating interactions between oceans and the atmosphere waves play an important role in the climate system [Hemer et al., 2012] and are likely to be affected by global warming. In several regions of the world, wave heights show already an upward trend in recent decades, especially the extremes [Wang et al., 2009; Young et al., 2011, 2012].

Regional impacts of climate change in coastal areas could be dominated by increased flooding and erosion from storm wave extremes, independent of relative sea level rise (RSLR) [Ruggiero, 2013; Barnard et al., 2015]. Yet the focus in literature when addressing future coastal impacts has been prevalently on the effects of RSLR [Hinkel et al., 2014]. The few global studies discussing large-scale projections of waves in view of climate change mainly focus on average wave conditions [Hemer et al., 2013a]. In global studies changes in extreme wave conditions have been marginally explored by focusing on high percentile values or on low return levels [Mori et al., 2010; Hemer et al., 2013a, 2013b; Semedo et al., 2013; Wang et al., 2014; Perez et al., 2015], omitting the rare extremes that may give rise to catastrophic impacts, although more detailed local studies exist [De Winter et al., 2012; Lionello et al., 2012; Casas-Prat and Sierra, 2013; Erikson et al., 2015; Shimura et al., 2016].

Studies based on satellite altimeter [Izaguirre et al., 2011] and reanalysis data [Dodet et al., 2010; Plomaritis et al., 2015; Kumar et al., 2016] revealed strong relationships between wind-wave climate and large-scale teleconnection patterns, such as the Antarctic Oscillation (AAO), the El Niño–Southern Oscillation (ENSO), and the North Atlantic Oscillation (NAO). Some of these indices are expected to intensify under increased anthropogenic forcing [Zheng et al., 2013; Cai et al., 2014], but it is not well understood how wind-wave variability and especially extreme waves will relate to these climate indices in a warmer world.

In this work we dynamically simulated the wave energy flux (WEF) with a global wave model driven by an ensemble of global coupled models (GCMs) from the Coupled Model Intercomparison Project Phase 5 (CMIP5) [Taylor et al., 2012] under the Representative Concentration Pathways scenario 8.5 [Meinshausen et al., 2011; van Vuuren et al., 2011]. We focused in particular on the 100 year return level of WEF, as a

proxy for coastal flooding and erosion, studying the long-term changes of its extremes estimated from a nonstationary extreme value analysis technique [Mentaschi *et al.*, 2016].

To explain the projected variations in extreme WEF, we investigated their correlation with long-term trends of climatic indices, such as the Antarctic Oscillation (AAO) index [Gong and Wang, 1999], often indicated also as Southern Annular Mode index in literature, the El Niño-Southern Oscillation (ENSO) index [Rasmusson and Wallace, 1983], and the North Atlantic Oscillation (NAO) index [Rodwell *et al.*, 1999]. These indices can be used to characterize the behavior of global and local geophysical systems, and are associated with the degree of instability of geophysical fluxes (like the jet streams or the thermohaline circulation) that induce extreme events and disasters, and are therefore useful to understand the consequences of climate changes.

2. Methods

The wave projections have been generated with the spectral wave model Wavewatch III (version 4.18 [Tolman, 2014]) forced by six CMIP5 models (for details see the supporting information and Perez *et al.* [2014]). In the wave model the source terms of growth/dissipation ST4 [Ardhuin *et al.*, 2010; Rascle and Ardhuin, 2013; Mentaschi *et al.*, 2015] was employed. The model setup consists of a global regular mesh with a resolution of 1.5°, spanning from latitude 80°S to 80°N, with nests on specific areas. The simulations were carried out on a 130 year time interval from 1970 to 2100 (for details see Vousdoukas *et al.* [2017]). The results of the simulations were saved for 4986 locations along the coast worldwide (Figure 1). For each location and each model, the wave energy flux (WEF, W/m) was computed as

$$\text{WEF} = E \cdot c_g = \frac{1}{64\pi} \rho g^2 T_{-10} H_s^2, \quad (1)$$

where E is the energy density (J/m^2), T_{-10} is the average period (s), and H_s is the significant wave height (m). A nonstationary extreme value analysis (EVA) was performed on each WEF time series by using the approach described by Mentaschi *et al.* [2016] in order to detect long-term trends in the extremes. The nonstationary EVA algorithm was set in order to filter out the variability on time scales below 30 years, to exclude from the analysis noise and sharp variations. The output of the EVA analysis was a location-specific time-varying generalized Pareto distribution for each WEF series, from which time-varying return levels were derived for specific return periods (50, 100, 200, and 500 years, focusing on the 100 year return level). The relative change of the N -year return levels of WEF was evaluated separately for each CMIP5 model. Then the absolute change of each model was computed applying its relative change to the ensemble return level of the historical scenario (see the supporting information). For each location the significance of the ensemble change in the 100 year return level of WEF was evaluated by means of the coefficient of variation CV_{2100} computed for the year 2100:

$$\text{CV}_{2100} = \frac{\sigma_{2100\text{WEF}}}{\langle \text{WEF}_{2100} - \text{WEF}_{\text{baseline}} \rangle}, \quad (2)$$

where $\langle \text{WEF}_{2100} - \text{WEF}_{\text{baseline}} \rangle$ is the ensemble average change between the end of the century and the baseline period and $\sigma_{2100\text{WEF}}$ is the intramodel standard deviation of WEF for the year 2100. The ensemble change in extreme WEF was considered significant if $|\text{CV}_{2100}| \leq 1$ [Alfieri *et al.*, 2015; Vousdoukas *et al.*, 2016a].

To investigate the correlation between extreme WEF and climatic indices a set of macroareas was selected in order to contain contiguous segments of coast with changes of extreme WEF of the same sign. The selected areas do not cover entirely the global coastline and have been arbitrarily identified so that each of them extends over a large area and contains a high percentage of points p_s with a significant and coherent trend, positive or negative. Therefore, important areas such as the northern Atlantic, the Yellow Sea, and the U.S. Pacific Coast were excluded from the correlation analysis because the majority of their locations do not present a significant ensemble change of extreme WEF. Other areas, such as the whole Indian Ocean, the Mediterranean Sea, and the British coast, were neither considered in the correlation analysis, because they contain subareas with opposite trends. This suggests that wave climate changes in these areas are characterized by a higher spatial variability, and that it would be difficult to connect them directly with the long-term intensification of large climatic patterns.

The climatic indices have been estimated as the first empirical orthogonal function of a principal component analysis of the anomalies of geophysical fields, such as the geopotential height (AAO and NAO) and the sea

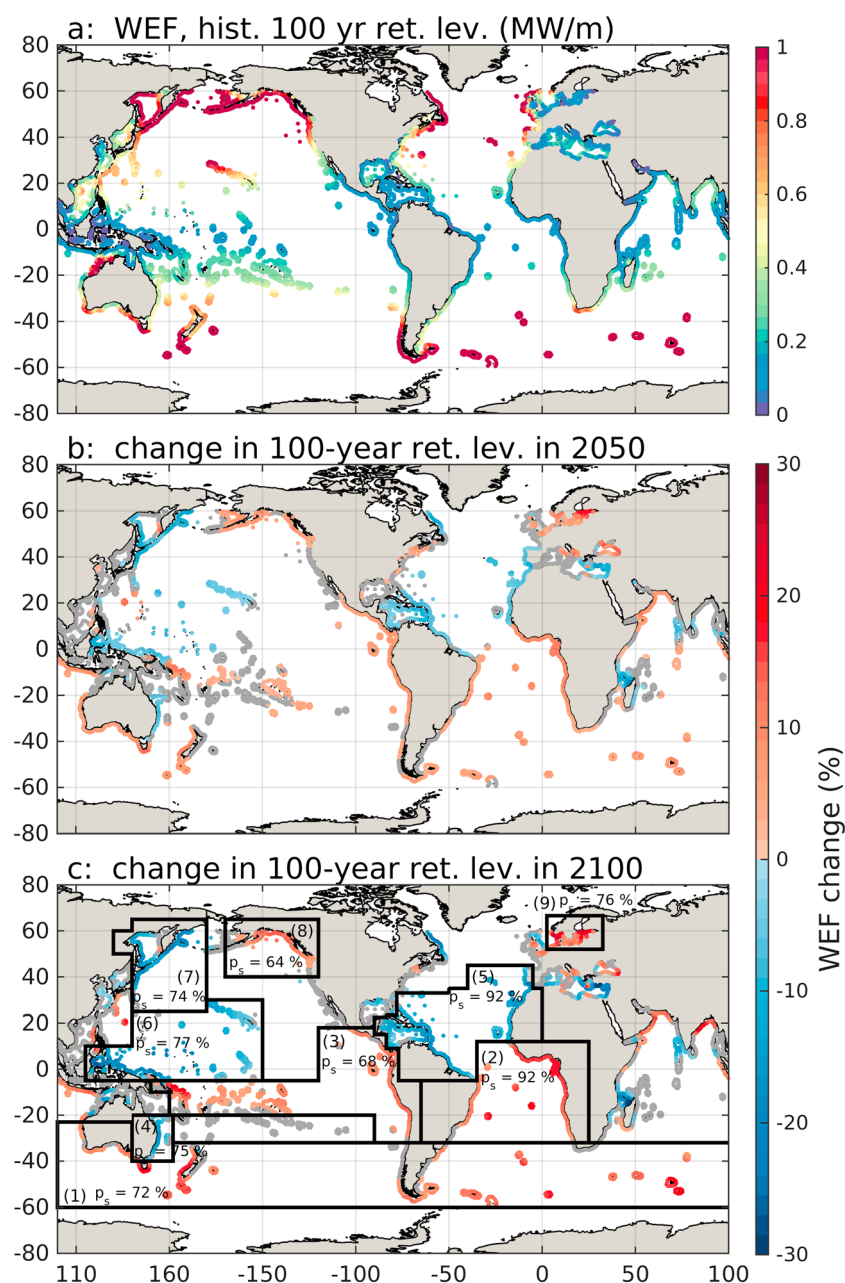


Figure 1. Ensemble projection of WEF along the global coastline: (a) baseline 100 year return level, ensemble relative change of the 100 year WEF for the year (b) 2050, and (c) 2100. The gray dots correspond to locations where no significant change was projected. In Figure 1c the areas of significant change are reported together with the percentage p_s of points where the increase is significant. The considered areas are the (1) southern temperate zone, (2) southern Atlantic, (3) subequatorial-tropical eastern Pacific, (4) eastern Australia, (5) northern tropical Atlantic, (6) north-western tropical Pacific, (7) north-western Pacific, (8) north-eastern Pacific, and (9) Baltic Sea.

surface temperature (ENSO). Since we are interested in long-term variations, the indices were low-pass filtered by means of a 30 years moving average.

For each model and area a correlation coefficient ρ was computed between the time-varying return level of WEF averaged over the area and the long-term change of a given climatic index. The ensemble correlation coefficient $\bar{\rho}$ was computed as the average of the correlations estimated for each CMIP5 model.

For all the locations the extreme wave direction was estimated as the mean direction of the waves beyond the 98.5 moving percentile of WEF. The ensemble difference between the directions of extreme WEF in

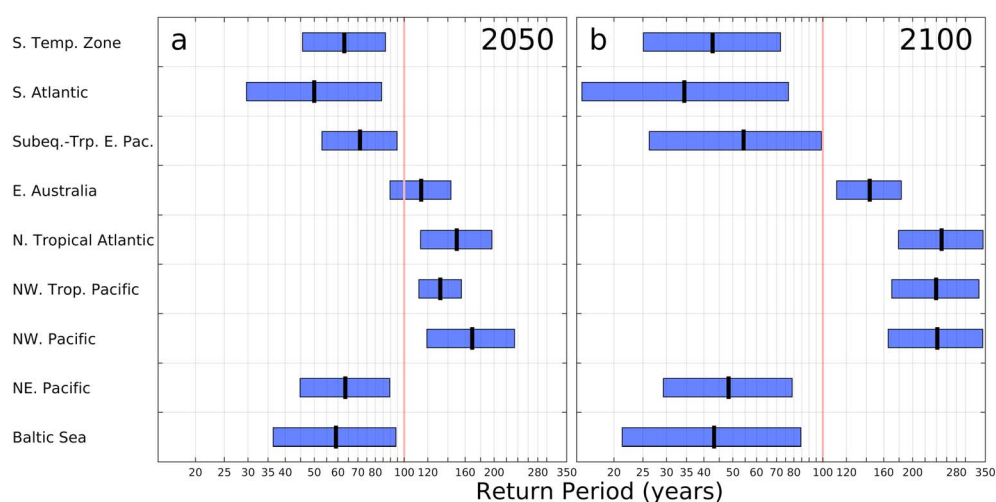


Figure 2. Projected return period of the present-day 100 year event (shown as vertical black line) for (a) 2050 and (b) 2100. The rows correspond to different areas, the black lines represent the projected return period, and the blue patches the confidence interval (defined by the intermodel standard deviation).

the time windows 2070–2100 and 1980–2010 was taken as the change in direction of extreme WEF. The ensemble change in direction $\Delta_e\theta$ was considered relevant for these locations where it exceeds the intermodel mean absolute deviation $MAD(\theta)$ of direction.

3. Results

The projected trend in the 100 year return level of WEF shows a remarkable variation between regions (Figure 1). A significant increase (decrease) in extreme WEF is projected by the end of this century along 29% (26%) of the global coastline. A significant increase of extreme WEF is projected along 43% of the Southern Hemisphere coastline, in particular for the whole southern temperate zone with the exception of Eastern Australia, the southern Atlantic, and the subequatorial-tropical eastern Pacific. In the Northern Hemisphere large coastal areas are characterized by a clear negative trend, including the northern tropical Atlantic, north-western tropical Pacific, and north-western Pacific. The north-eastern Pacific and Baltic Sea, on the other hand, show positive trends, with rises up to 30%, in extreme WEF.

The relative changes found for the 50, 200, and 500 year return levels (see Table S1 in the supporting information) appear to increase slightly with the return levels, and the increase for more exceptional events is consistently larger than the changes found for the mean WEF. The average change of the 100 year return level at the locations where we find increase (decrease) is of about 12.5% (–13%), while the average change of the mean WEF is 5.48% (–6.83%). This finding is in line with previous studies based on historical data [Young *et al.*, 2011]. Moreover, similar relative changes of different return levels involve higher absolute changes of power for more extreme events. In particular, the increase (decrease) of power of the 500 year extreme is on average 37% higher (61% lower) than the one of the 50 year extreme.

The increase in WEF projected along several areas (southern temperate zone, southern Atlantic, subequatorial-tropical eastern Pacific, north-eastern Pacific, and Baltic Sea) translates into an increase in frequency (Figure 2), with the present-day 100 year event being projected to occur at least every 50 years, towards the end of the century. A smaller increase in frequency was projected along the subequatorial-tropical eastern Pacific, where the present-day event of the century occurs every 54 years in 2100. Conversely, the projected decrease in WEF in other areas is expressed also in a more than 50% reduction of the frequency towards the end of the century. Eastern Australia is an exception as the present-day event of the century is projected to occur every 150 years.

The changes of extreme WEF projected for 2050 present spatial patterns similar to the ones projected for 2100, but the variation is smaller in both magnitude and frequency (Figures 1 and 2), with absolute changes in magnitude always below 20% and absolute changes in frequency below 50%.

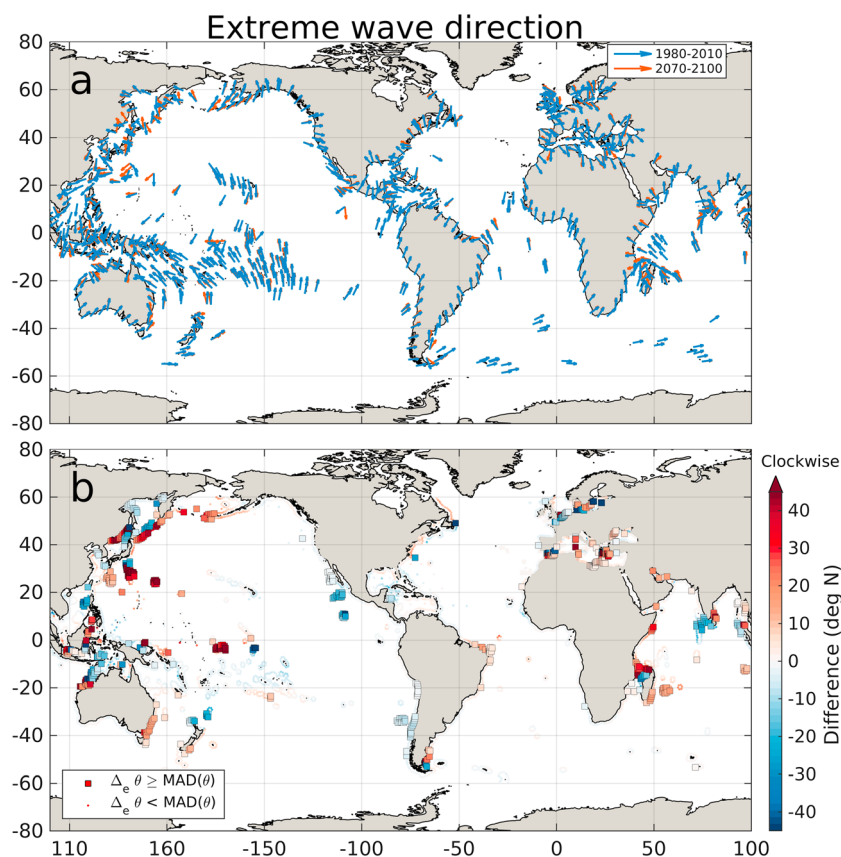


Figure 3. Ensemble mean change of extreme WEF direction: (a) quiver plots showing the direction of propagation for the baseline and 2070–2100. (b) Scatterplot showing the direction change between the start and end of the century, expressed by the box color; the box type indicates that the change in direction exceeds the intermodel MAD of the change.

In many locations the direction of extreme WEF is projected to change significantly by the end of the century (Figure 3), with variations in some cases of tens of degrees, in some locations of the north-western Pacific, of the equatorial Pacific, of north-western Australia, and in the area north-west of Madagascar. In the majority of the locations of the Southern Hemisphere we projected a northward rotation of extreme WEF, except for Eastern Australia and a few other areas sheltered from the Southern Ocean swell. In the majority of the locations of the northern temperate zone we projected an eastward rotation of extreme WEF.

4. Discussion

The projected changes are for many regions qualitatively similar to those for the 10 year return level obtained by Wang *et al.* [2014] using statistical modeling. The magnitude of the changes presented herein are generally more pronounced in both directions, and this is consistent with the employment in this study of the WEF, that is proportional to $H_s^2 \cdot T$, while Wang *et al.* [2014] studied the 10 year return level of H_s . The present projections show an overall stronger statistical significance, partially due to the nonstationary extreme value analysis, which allows for bigger samples and consequently less statistical fitting uncertainty, compared to a stationary approach applied on time slices [Mentaschi *et al.*, 2016]. Moreover, dynamical models allow for a more accurate representation of extreme conditions compared to statistical methodologies, due to the scarce availability of extreme data to train the statistical models [Breivik *et al.*, 2014; Laugel *et al.*, 2014; Martínez-Asensio *et al.*, 2014].

To explain the projected changes of extreme WEF, we studied their correlation with the long-term tendencies of the AAO, NAO, and ENSO indices. Some aspects of the complex dynamics related to these indices are not yet fully understood and represented by GCMs [Davini and Cagnazzo, 2013; Kim and Cai, 2014; Yeo and Kim, 2015]. Yet the CMIP5 models are able to catch their basic features both in terms of shape and percentage of

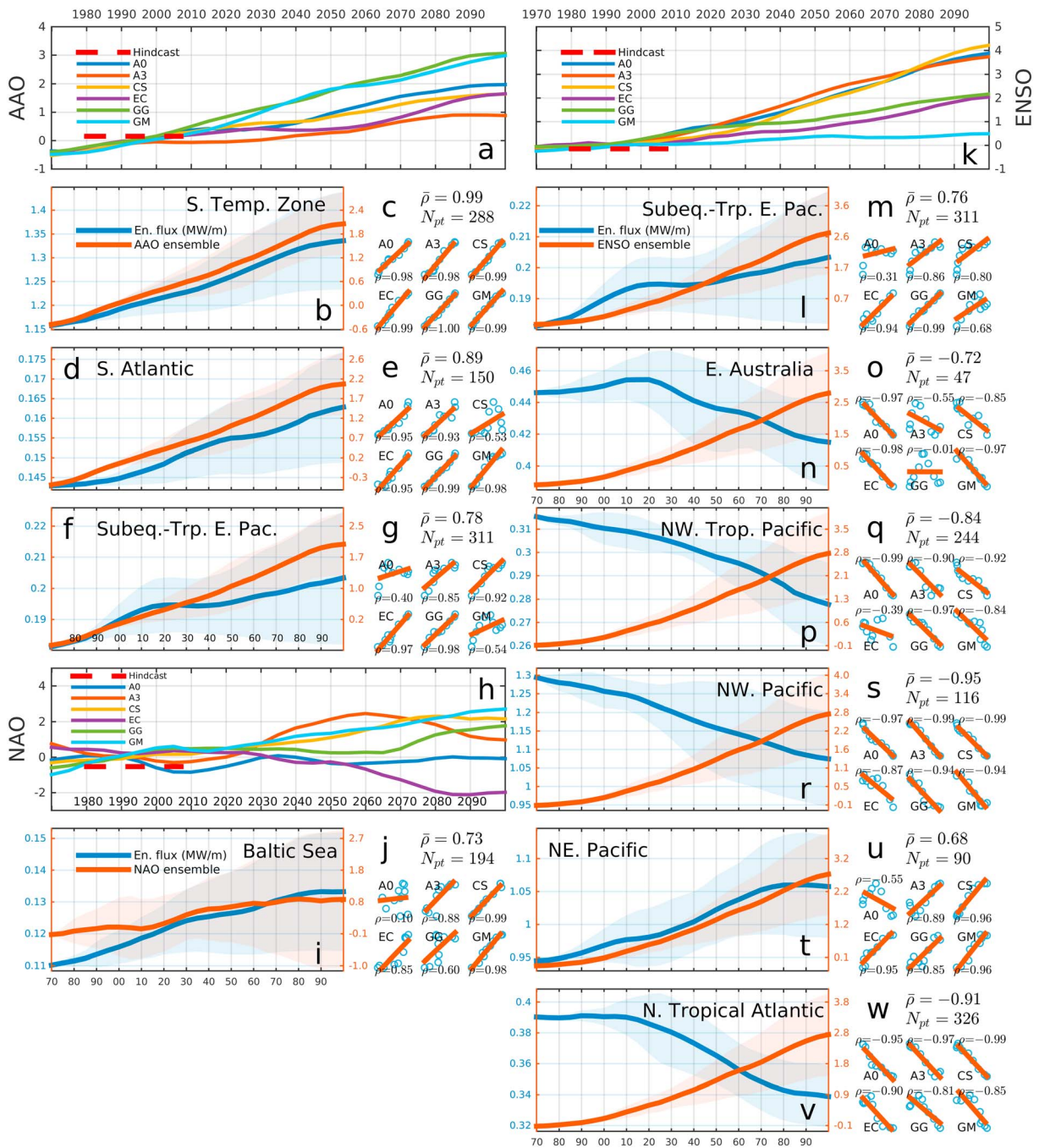


Figure 4. Projected long-term trend of (a) AAO, (h) NAO, and (k) ENSO indices. The dashed thick red line indicates the index estimated for ERA-Interim. (b, d, f, i, l, n, p, r, t, and v) Comparisons of one of the ensemble indices (b, e, and f: AAOI; i: NAO, and n–v: ENSO) with the ensemble 100 year WEF for different regions. (c, e, g, j, m, o, q, s, u, and w) Scatterplots and the correlation coefficients ρ between the AAO index (Figures 4c, 4e, and 4g) or the NAO index (Figure 4j) or the ENSO index (Figures 4q, 4s, 4u, and 4w) and the 100 year return level of WEF for each of the CMIP5 models and for the respective regions. The average correlation coefficient $\bar{\rho}$ and the number of points N_{pt} of the area are also reported.

explained variance, i.e., the weight of the pattern to the total climatic variability [Lee and Black, 2013; Zheng et al., 2013; Cai et al., 2014]. Projections along the 21st century show a significant long-term increase of AAO (Figure 4a) characterized by an intensification of the AAO pattern. The low pressure over Antarctica is expected to deepen, and the meridional thermal gradient at high latitudes in the Southern Hemisphere is expected to strengthen, with a consequent poleward shift of the storm tracks [Arblaster et al., 2011; Zheng et al., 2013]. This is coherent with the increase of extreme WEF projected for the Southern Hemisphere

(Figures 4b–4g), with the exception of Eastern Australia and a few other areas sheltered from swell from the Southern Ocean. The positive correlation is particularly significant in the southern temperate zone, where the ensemble average correlation coefficient $\bar{\rho}$ is very close to 1 ($\bar{\rho} = 0.99$). This confirms that AAO has a strong influence on the climate of the Southern Hemisphere. Especially at high latitudes a positive phase of AAO is associated with an intensification of the meridional thermal gradient and of the inherent baroclinic instability [Mo, 2000; Gupta and England, 2006] that generates storms and extreme winds related to extreme waves. The increase of extreme WEF at lower latitudes in the Southern Hemisphere, in the southern Atlantic, and in the subequatorial-tropical eastern Pacific can also be connected with the long-term variation of AAO. This is partly due to an increase of the swell coming from the Southern Ocean that also explains the equatorward rotation of extreme WEF projected by the end of the XXI century in many areas of the Southern hemisphere (Figure 3). On the other hand, an intensified AAO can be associated with a warming sea surface at subtropical latitudes, involving more intense convection and more frequent storms [Grassi *et al.*, 2005].

In a way similar to AAO for the Southern Ocean, the NAO index is a proxy for the meridional thermal gradient in the northern Atlantic. A high NAO phase corresponds to a northward shift and an intensification of storm tracks over northern Europe [Rodwell *et al.*, 1999]. This explains the good correlation between the long-term variations of the NAO index and the change of extreme WEF in the Baltic Sea (Figures 4i and 4j), because a stronger NAO is associated with more powerful and unstable westerlies and with an enforced storm activity that leads to more intense extreme waves [Hurrell, 1995]. Conditions of more intense westerlies over the Baltic Sea can also explain the eastward rotation of the extreme WEF in this area (Figure 3). Although we find a strong correlation between the long-term changes of NAO and of extreme WEF, the weaker and more uncertain intensification of NAO (Figure 4h) does not fully explain the robust increase of extreme WEF in the Baltic Sea. The disagreement within the model ensemble about the trend of NAO can be connected to the absence of a significant change of extreme WEF in wide portions of the northern Atlantic coasts.

ENSO shows a significant tendency to increase (Figure 4k) expressed by an intensification of the ENSO pattern and a shift of climate toward El Niño conditions [Cai *et al.*, 2014]. This indicates a warming of the Peruvian upwelling zone and a strengthened thermal gradient to the western side of the Pacific Ocean, while the jet stream in the Northern Hemisphere is expected to shift southward [Philander, 1983]. The geophysical dynamics related to ENSO are complex and have vast consequences worldwide [Cai *et al.*, 2014]. The warm temperature anomalies of the Peruvian upwelling zone during El Niño enforce convective motions and cause a strengthened instability in the equatorial eastern Pacific, resulting in more intense and frequent storms and extreme winds and subsequently waves [Philander, 1983; Rasmusson and Wallace, 1983; Timmerman *et al.*, 1999; Jin *et al.*, 2014]. This explains the significant positive correlation between the projected long-term variation of ENSO and the increase of extreme WEF in the subequatorial-tropical eastern Pacific (Figures 4l and 4m). We note that CMIP5 models present some shortcomings in the simulation of tropical cyclones that dominate the extreme WEF in areas such as the subequatorial-tropical eastern Pacific, usually modeling features weaker, larger, and less frequent than observed, and underestimating the peaks mainly due to the low resolution [Camargo, 2013] and to the lack of ocean-atmosphere coupling in many CMIP5 models [Shimura *et al.*, 2016]. Moreover, the complex coupled dynamics of tropical cyclones and waves are not yet fully understood [Babanin *et al.*, 2012; Toffoli *et al.*, 2012; Chen *et al.*, 2013; Janssen *et al.*, 2013; Zappa *et al.*, 2016]. However, they are designed to model properly the large features of geophysical fields that impact on the intensity and frequency of the tropical cyclones [Camargo, 2013]. In addition, a strong connection between positive ENSO phases and more frequent and intense tropical cyclones in the tropical eastern Pacific is well documented [Jin *et al.*, 2014]. Therefore, the increase of the extreme WEF projected with the CMIP5 models for the subequatorial-tropical eastern Pacific and for other tropical regions can be considered a proxy of an increase of the extreme WEF associated with full-scale tropical cyclones.

El Niño conditions are also generally associated with a strengthening of the Aleutian low and of high pressures west of the Rocky Mountains [Philander, 1983; Barnard *et al.*, 2015]. This enforces the winds over north-western Canada and Alaska, explaining why the long-term increase of ENSO is correlated with the growth of extreme WEF along the north-eastern Pacific coasts (Figures 4t and 4u). This mechanism also explains the eastward rotation of extreme WEF in many locations in the northern Pacific (Figure 3) [Raible *et al.*, 2005]. For many other regions the intensification of ENSO will result in less extreme wave climate. Along the coasts of the western Pacific and in Eastern Australia (Figures 4n and 4o) the inverse correlation is consistent with colder and dryer conditions in Eastern Asia and Eastern Australia during El Niño episodes,

with reduced cyclonic activity and consequently less frequent storms and extreme winds and waves [Power *et al.*, 1999; Wang *et al.*, 2000; Verdon *et al.*, 2004]. In the north-western Pacific, a progressive shift southward of the jet stream and of the storm-tracks under El Niño conditions results in a colder and more stable climate [Wang *et al.*, 2000; Barnard *et al.*, 2015], exemplified by strong negative correlation between the trends in extreme WEF and the ENSO index ($\bar{\rho} = -0.95$). A rather strong negative correlation is also observed for the northern tropical Atlantic ($\bar{\rho} = -0.91$; Figures 4v and 4w). There is evidence from historical data of a robust teleconnection of El Niño with the northern tropical Atlantic [Chang *et al.*, 2006]. Although the mechanism is not yet fully understood, a possible explanation is that a warmer-than-the-average northern tropical Atlantic can induce a low-level atmospheric flow over eastern Pacific, triggering La Niña conditions [Ham *et al.*, 2013]. Conversely, El Niño conditions are generally associated to cooler-than-the-average and more stable conditions in the northern tropical Atlantic, with less intense and frequent storms and extreme waves.

The projected changes of extreme WEF can lead to increased coastal impacts, especially along low-lying, densely populated, and often scarcely protected coastal areas along the Southern Hemisphere, where an increase of extreme WEF is projected. For example, extreme WEF is projected to increase by 25% along the Guinea Gulf (western Africa), and the present-day 100 year event is expected to more than double in frequency toward the end of the century, while the area is already experiencing coastal erosion and inundation issues [French *et al.*, 1995; Odunuga *et al.*, 2014]. Such an increase, combined with anticipated RSLR of 0.5–1.5 m [Church *et al.*, 2013; Hinkel *et al.*, 2014], and fast-growing population trends [Zinkina and Korotayev, 2014], can lead to higher wave-induced water levels, energy, and thus coastal impacts. Small Island Developing States located in the tropical southern Pacific are known for their limited and low-lying areas and their strong exposure to coastal hazard [Strolazzi *et al.*, 2011; Duvat *et al.*, 2013]. An increase of extreme WEF of about 10% by the end of the century, together with the effects of RSLR, could compromise a significant portion of their surface and even threaten the existence of some atolls.

On the other hand, the projected decrease in extreme WEF along other parts of the world could partially counterbalance RSLR and related impacts, highlighting the need to assess all hazard components in view of climate change in order to have the full picture of future risks.

5. Conclusions

The extreme WEF along the coast worldwide is projected to change significantly by the end of the century. In the Southern Hemisphere the change is positive in 43% of the examined locations, with an increase of the 100 year return level of ~15%. A significant decrease of extreme WEF is instead projected along most of the Northern Hemisphere, with the exception of the north-eastern Pacific (with an average increase of ~10%), and the Baltic Sea (~20% on average, with maxima up to 30%).

The changes in magnitude translate into considerable changes in the recurrence frequency of extreme events, which are projected to occur twice as frequently along many areas, especially in the Southern Hemisphere. The latter could imply an intensification of coastal erosion and wave-induced impacts.

In many areas the changes of extreme WEF can be explained as a consequence of a long-term intensification of climatic patterns such as AAO, ENSO, and, to a lesser extent, NAO. The link between the long-term variations of the climatic indices and the change of extreme WEF is, in general, strong for all the models of the ensemble, along all the considered areas, and is particularly significant in the southern temperate zone, where the average correlation between the AAO index and the change of extreme WEF is 0.99; the southern Atlantic, where the correlation with the AAO index is 0.89; the north-western Pacific, where the correlation with the ENSO index is -0.95 ; and the northern tropical Atlantic, where the correlation with the ENSO index is -0.91 .

References

- Alfieri, L., P. Burek, L. Feyen, and G. Forzieri (2015), Global warming increases the frequency of river floods in Europe, *Hydrol. Earth Syst. Sci.*, 19(5), 2247–2260.
- Arblaster, J. M., G. A. Meehl, and D. J. Karoly (2011), Future climate change in the Southern Hemisphere: Competing effects of ozone and greenhouse gases, *Geophys. Res. Lett.*, 38, L02701, doi:10.1029/2010GL045384.
- Archetti, R., A. Paci, S. Carniel, and D. Bonaldo (2016), Optimal index related to the shoreline dynamics during a storm: The case of Jesolo beach, *Nat. Hazards Earth Syst. Sci.*, 16(5), 1107–1122, doi:10.5194/nhess-16-1107-2016.

Acknowledgments

This research received funding from the EU Seventh Framework Programme FP7/2007–2013 under grant agreement 603864 (‘‘High-End cLimate Impacts and eXtremes’’; www.helixclimate.eu) and from the JRC of the European Commission as part of the CoastAlRisk and ADAPTATION projects. Support from CAPES for Special Visiting Professor (PVE) under the project 88881.068343/2014-01 is also acknowledged. The data set illustrated in this paper is available through the JRC open access database from this link: <http://data.jrc.ec.europa.eu/collection/LISCOAST>.

- Arduhin, F., et al. (2010), Semiempirical dissipation source functions for ocean waves. Part I: Definition, calibration, and validation, *J. Phys. Oceanogr.*, *40*(9), 1917–1941.
- Babanin, A. V., M. Onorato, and F. Qiao (2012), Surface waves and wave-coupled effects in lower atmosphere and upper ocean, *J. Geophys. Res.*, *117*, C00J01, doi:10.1029/2012JC007932.
- Barnard, P. L., et al. (2015), Coastal vulnerability across the Pacific dominated by El Niño/Southern Oscillation, *Nat. Geosci.*, *8*(10), 801–807, doi:10.1038/ngeo2539.
- Bertin, X., N. Bruneau, J. F. Breilh, A. B. Fortunato, and M. Karpytchev (2012), Importance of wave age and resonance in storm surges: The case Xynthia, Bay of Biscay, *Ocean Model.*, *42*, 16–30, doi:10.1016/j.ocemod.2011.11.001.
- Breivik, Ø., O. J. Aarnes, S. Abdalla, J. R. Bidlot, and P. A. E. M. Janssen (2014), Wind and wave extremes over the world oceans from very large ensembles, *Geophys. Res. Lett.*, *41*, 5122–5131, doi:10.1002/2014GL060997.
- Cai, W., et al. (2014), Increasing frequency of extreme El Niño events due to greenhouse warming, *Nat. Clim. Change*, *5*(2), 1–6, doi:10.1038/nclimate2100.
- Camargo, S. J. (2013), Global and regional aspects of tropical cyclone activity in the CMIP5 models, *J. Clim.*, *26*(24), 9880–9902, doi:10.1175/JCLI-D-12-00549.1.
- Casas-Prat, M., and J. P. Sierra (2013), Projected future wave climate in the NW Mediterranean Sea, *J. Geophys. Res. Oceans*, *118*, 3548–3568, doi:10.1002/jgrc.20233.
- Chang, P., Y. Fang, R. Saravanan, L. Ji, and H. Seidel (2006), The cause of the fragile relationship between the Pacific El Niño and the Atlantic Niño, *Nature*, *443*(7109), 324–328, doi:10.1038/nature05053.
- Chen, S. S., W. Zhao, M. A. Donelan, H. L. Tolman, S. S. Chen, W. Zhao, M. A. Donelan, and H. L. Tolman (2013), Directional wind–wave coupling in fully coupled atmosphere–wave–ocean models: Results from CBLAST-hurricane, *J. Atmos. Sci.*, *70*(10), 3198–3215, doi:10.1175/JAS-D-12-0157.1.
- Church, J. A., et al. (2013), Sea level change, in *Climate Change 2013: The Physical Science Basis. Contribution of Working Group I to the Fifth Assessment Report of the Intergovernmental Panel on Climate Change*, edited by T. F. Stocker et al., pp. 1137–1216, Cambridge Univ. Press, Cambridge, U. K., and New York.
- Davini, P., and C. Cagnazzo (2013), On the misinterpretation of the North Atlantic Oscillation in CMIP5 models, *Clim. Dyn.*, *43*, 1497–1511, doi:10.1007/s00382-013-1970-y.
- De Winter, R. C., A. Sterl, J. W. De Vries, S. L. Weber, and G. Ruessink (2012), The effect of climate change on extreme waves in front of the Dutch coast, *Ocean Dyn.*, *62*(8), 1139–1152, doi:10.1007/s10236-012-0551-7.
- Dodet, G., X. Bertin, and R. Taborda (2010), Wave climate variability in the North-East Atlantic Ocean over the last six decades, *Ocean Model.*, *37*(3–4), 120–131, doi:10.1016/j.ocemod.2009.10.010.
- Duvat, V., A. Magnan, and F. Pouget (2013), Exposure of atoll population to coastal erosion and flooding: A South Tarawa assessment, Kiribati, *Sustain. Sci.*, *8*(3), 423–440, doi:10.1007/s11625-013-0215-7.
- Erikson, L. H., C. A. Heggermiller, P. L. Barnard, P. Ruggiero, and M. van Ormondt (2015), Projected wave conditions in the Eastern North Pacific under the influence of two CMIP5 climate scenarios, *Ocean Model.*, *96*, 171–185, doi:10.1016/j.ocemod.2015.07.004.
- French, G. T., L. F. Awosika, and C. E. Ibe (1995), Sea-level rise and Nigeria: Potential impacts and consequences, *J. Coast. Res.*, *14*, 224–242.
- Gong, D., and S. Wang (1999), Definition of Antarctic oscillation index, *Geophys. Res. Lett.*, *26*, 459–462, doi:10.1029/1999GL000003.
- Grassi, B., G. Redaelli, and G. Visconti (2005), Simulation of Polar Antarctic trends: Influence of tropical SST, *Geophys. Res. Lett.*, *32*, L23806, doi:10.1029/2005GL023804.
- Gupta, A. S., and M. H. England (2006), Coupled ocean-atmosphere-ice response to variations in the southern annular mode, *J. Clim.*, *19*(18), 4457–4486, doi:10.1175/JCLI3843.1.
- Ham, Y.-G., J.-S. Kug, J.-Y. Park, and F.-F. Jin (2013), Sea surface temperature in the north tropical Atlantic as trigger for El Niño/Southern Oscillation events, *Nat. Geosci.*, *6*, 112–116.
- Hemer, M. A., X. L. Wang, R. Weisse, and V. R. Swail (2012), Advancing wind-waves climate science: The COWCLIP project, *Bull. Am. Meteorol. Soc.*, *93*(6), 791–796.
- Hemer, M. A., Y. Fan, N. Mori, A. Semedo, and X. L. Wang (2013a), Projected changes in wave climate from a multi-model ensemble, *Nat. Clim. Change*, *3*(5), 471–476, doi:10.1038/nclimate1791.
- Hemer, M. A., J. Katzfey, and C. E. Trenham (2013b), Global dynamical projections of surface ocean wave climate for a future high greenhouse gas emission scenario, *Ocean Model.*, *70*, 221–245, doi:10.1016/j.ocemod.2012.09.008.
- Hinkel, J., D. Lincke, A. T. Vafeidis, M. Perrette, R. J. Nicholls, R. S. J. Tol, B. Marzeion, X. Fettweis, C. Ionescu, and A. Levermann (2014), Coastal flood damage and adaptation costs under 21st century sea-level rise, *Proc. Natl. Acad. Sci. U.S.A.*, *111*(9), 3292–3297, doi:10.1073/pnas.1222469111.
- Hurrell, J. W. (1995), Decadal trends in the North Atlantic oscillation: Regional temperatures and precipitation, *Science*, *269*(5224), 676–679, doi:10.1126/science.269.5224.676.
- Izaguirre, C., F. J. Méndez, M. Menéndez, and I. J. Losada (2011), Global extreme wave height variability based on satellite data, *Geophys. Res. Lett.*, *38*, L10607, doi:10.1029/2011GL047302.
- Janssen, P. A. E. M., Ø. Breivik, K. Mogensen, F. Vitart, M. Balmaseda, J.-R. Bidlot, S. Keeley, M. Leutbecher, L. Mangusson, and F. Molteni (2013), Air-sea interaction and surface waves, *ECMWF Tech. Mem.*, *712*.
- Jin, F.-F., J. Boucharel, and I.-I. Lin (2014), Eastern Pacific tropical cyclones intensified by El Niño delivery of subsurface ocean heat, *Nature*, *516*(7529), 82–85, doi:10.1038/nature13958.
- Kim, W. M., and W. Cai (2014), The importance of the eastward zonal current for generating extreme El Niño, *Clim. Dyn.*, *42*(11–12), 3005–3014, doi:10.1007/s00382-013-1792-y.
- Kumar, P., S.-K. Min, E. Weller, H. Lee, and X. L. Wang (2016), Influence of climate variability on extreme ocean surface wave heights assessed from ERA-interim and ERA-20C, *J. Clim.*, *29*(11), 4031–4046.
- Laugel, A., M. Menendez, M. Benoit, G. Mattarolo, and F. Méndez (2014), Wave climate projections along the French coastline: Dynamical versus statistical downscaling methods, *Ocean Model.*, *84*, 35–50, doi:10.1016/j.ocemod.2014.09.002.
- Lee, Y. Y., and R. X. Black (2013), Boreal winter low-frequency variability in CMIP5 models, *J. Geophys. Res. Atmos.*, *118*, 6891–6904, doi:10.1002/jgrd.50493.
- Lionello, P., M. B. Galati, and E. Elvini (2012), Extreme storm surge and wind wave climate scenario simulations at the Venetian littoral, *Phys. Chem. Earth*, *40–41*, 86–92, doi:10.1016/j.pce.2010.04.001.
- Martínez-Asensio, A., M. Marcos, M. N. Tsimplis, G. Jordà, X. Feng, and D. Gomis (2014), On the ability of statistical wind-wave models to capture the variability and long-term trends of the North Atlantic winter wave climate, *Ocean Model.*, doi:10.1016/j.ocemod.2016.02.006.

- Masselink, G., and J. A. Puleo (2006), Swash-zone morphodynamics, *Cont. Shelf Res.*, 26(5), 661–680, doi:10.1016/j.csr.2006.01.015.
- Masselink, G., B. Castelle, T. Scott, G. Dodet, S. Suanez, D. Jackson, and F. Floc'h (2016), Extreme wave activity during 2013/2014 winter and morphological impacts along the Atlantic coast of Europe, *Geophys. Res. Lett.*, 43, 2135–2143, doi:10.1002/2015GL067492.
- Matias, A., Ó. Ferreira, A. Vila-Concejo, T. Garcia, and J. A. Dias (2008), Classification of washover dynamics in barrier islands, *Geomorphology*, 97(3–4), 655–674, doi:10.1016/j.geomorph.2007.09.010.
- Meinshausen, M., et al. (2011), The RCP greenhouse gas concentrations and their extensions from 1765 to 2300, *Clim. Change*, 109(1), 213–241, doi:10.1007/s10584-011-0156-z.
- Mentaschi, L., G. Besio, F. Cassola, and A. Mazzino (2015), Performance evaluation of WavewatchIII in the Mediterranean Sea, *Ocean Model.*, 90, 82–94.
- Mentaschi, L., M. Voudoukas, E. Voukouvalas, L. Sartini, L. Feyen, G. Besio, and L. Alfieri (2016), The transformed-stationary approach: A generic and simplified methodology for non-stationary extreme value analysis, *Hydrol. Earth Syst. Sci.*, 20(9), 3527–3547, doi:10.5194/hess-20-3527-2016.
- Mo, K. C. (2000), Relationships between low-frequency variability in the Southern Hemisphere and sea surface temperature anomalies, *J. Clim.*, 13(20), 3599–3610, doi:10.1175/1520-0442(2000)013<3599:RBLFVI>2.0.CO;2.
- Monioudi, I. N. (2016), Assessment of island beach erosion due to sea level rise: The case of the Aegean Archipelago (Eastern Mediterranean), *Nat. Hazards Earth Syst. Sci. Discuss.*, doi:10.5194/nhess-2016-336.
- Mori, N., T. Yasuda, H. Mase, T. Tom, and Y. Oku (2010), Projection of extreme wave climate change under global warming, *Hydrol. Res. Lett.*, 4, 15–19, doi:10.3178/hrl.4.15.
- Ogunuga, S., G. Badru, and O. M. Bello (2014), Climate change, sea level rise and coastal inundation along part of Nigeria Barrier Lagoon Coast, *J. Appl. Sci. Environ. Manage.*, 18, 41–47.
- Oumeraci, H. (1994), Review and analysis of vertical breakwater failures—Lessons learned, *Coast. Eng.*, 22(1–2), 3–29, doi:10.1016/0378-3839(94)90046-9.
- Perez, J., M. Menendez, F. J. Mendez, and I. J. Losada (2014), Evaluating the performance of CMIP3 and CMIP5 global climate models over the north-east Atlantic region, *Clim. Dyn.*, 1–18, doi:10.1007/s00382-014-2078-8.
- Perez, J., M. Menendez, P. Camus, F. Mendez, and I. J. Losada (2015), Statistical multi-model climate projections of surface ocean waves in Europe, *Ocean Model.*, 96, 161–170.
- Philander, S. G. H. (1983), El Niño Southern Oscillation phenomena, *Nature*, 302, 295–301, doi:10.1038/302295a0.
- Plomaritis, T. A., J. Benavente, I. Laiz, and L. Del Rio (2015), Variability in storm climate along the Gulf of Cadiz: The role of large scale atmospheric forcing and implications to coastal hazards, *Clim. Dyn.*, 45, 2499–2514.
- Postacchini, M., L. Soldini, C. Lorenzoni, and A. Mancinelli (2017), Medium-term dynamics of a Middle Adriatic barred beach, *Ocean Sci. Discuss.*, doi:10.5194/os-2016-106.
- Power, S., T. Casey, C. Folland, A. Colman, and V. Mehta (1999), Inter-decadal modulation of the impact of ENSO on Australia, *Clim. Dyn.*, 15(5), 319–324, doi:10.1007/s003820050284.
- Raible, C. C., T. F. Stocker, M. Yoshimori, M. Renold, U. Beyerle, C. Casty, and J. Luterbacher (2005), Northern hemispheric trends of pressure indices and atmospheric circulation patterns in observations, reconstructions, and coupled GCM simulations, *J. Clim.*, 18(19), 3968–3982, doi:10.1175/JCLI3511.1.
- Raschle, N., and F. Ardhuin (2013), A global wave parameter database for geophysical applications. Part 2: Model validation with improved source term parameterization, *Ocean Model.*, 70, 174–188, doi:10.1016/j.ocemod.2012.12.001.
- Rasmusson, E. M., and J. M. Wallace (1983), Meteorological aspects of the El Niño/Southern Oscillation, *Science*, 222(4629), 1195–1202, doi:10.1126/science.222.4629.1195.
- Rodwell, M. J., D. P. Rowell, and C. K. Folland (1999), Oceanic forcing of the wintertime North Atlantic Oscillation and European climate, *Nature*, 398(6725), 320–323, doi:10.1038/18648.
- Roelvink, D., A. Reniers, A. van Dongeren, J. van Thiel de Vries, R. McCall, and J. Lescinski (2009), Modelling storm impacts on beaches, dunes and barrier islands, *Coast. Eng.*, 56(11–12), 1133–1152, doi:10.1016/j.coastaleng.2009.08.006.
- Ruggiero, P. (2013), Is the intensifying wave climate of the U. S. Pacific Northwest increasing flooding and erosion risk faster than sea-level rise?, *J. Waterw. Port, Coastal, Ocean Eng.*, 139, 88–97, doi:10.1061/(ASCE)WW.1943-5460.0000172.
- Semedo, A., R. Weisse, A. Behrens, A. Sterl, L. Bengtsson, and H. Günther (2013), Projection of global wave climate change toward the end of the twenty-first century, *J. Clim.*, 26(21), 8269–8288, doi:10.1175/JCLI-D-12-00658.1.
- Shimura, T., N. Mori, and M. A. Hemer (2016), Projection of tropical cyclone-generated extreme wave climate based on CMIP5 multi-model ensemble in the Western North Pacific, *Clim. Dyn.*, 14, 1–14.
- Stockdon, H. F., R. A. Holman, P. A. Howd, and A. H. Sallenger (2006), Empirical parameterization of setup, swash, and runup, *Coast. Eng.*, 53(7), 573–588, doi:10.1016/j.coastaleng.2005.12.005.
- Strolazzi, C. D., E. Elias, M. E. Field, and M. K. Presto (2011), Numerical modelling of the impact of sea-level rise on fringing coral reef hydrodynamics and sediment transport, *Coral Reefs*, 30, 83–96.
- Taylor, K. E., R. J. Stouffer, and G. A. Meehl (2012), An overview of CMIP5 and the experiment design, *Bull. Am. Meteorol. Soc.*, 93(4), 485–498, doi:10.1175/BAMS-D-11-00094.1.
- Timmerman, A., J. Oberhuber, A. Bacher, M. Esch, M. Latif, and E. Roeckner (1999), Increased El Niño frequency in a climate model forced by future greenhouse warming, *Nature*, 398, 694–697, doi:10.1038/19505.
- Toffoli, A., J. D. McConochie, M. Ghantous, L. Loffredo, and A. V. Babanin (2012), The effect of wave-induced turbulence on the ocean mixed layer during tropical cyclones: Field observations on the Australian North-West Shelf, *J. Geophys. Res.*, 117, C00J24, doi:10.1029/2011JC007780.
- Tolman, H. L. (2014), User manual and system documentation of WAVEWATCH III version 4.18.
- Van der Meer, J. W., N. W. H. Allsop, T. Bruce, J. De Rouck, A. Kortenhaus, T. Pullen, H. Schüttrumpf, P. Troch, and B. Zanuttigh (2016), Manual on wave overtopping of sea defences and related structures.
- van Vuuren, D. P., et al. (2011), The representative concentration pathways: An overview, *Clim. Change*, 109(1), 5–31, doi:10.1007/s10584-011-0148-z.
- Verdon, D. C., A. M. Wyatt, A. S. Kiem, and S. W. Franks (2004), Multidecadal variability of rainfall and streamflow: Eastern Australia, *Water Resour. Res.*, 40, W10201, doi:10.1029/2004WR003234.
- Voudoukas, M. I., L. P. M. Almeida, and Ó. Ferreira (2012a), Beach erosion and recovery during consecutive storms at a steep-sloping, meso-tidal beach, *Earth Surf. Process. Landforms*, 37(6), 583–593, doi:10.1002/esp.2264.
- Voudoukas, M. I., D. Wziatek, and L. P. Almeida (2012b), Coastal vulnerability assessment based on video wave run-up observations at a mesotidal, steep-sloped beach, *Ocean Dyn.*, 62(1), 123–137, doi:10.1007/s10236-011-0480-x.

- Vousdoukas, M. I., E. Voukouvalas, A. Annunziato, A. Giardino, and L. Feyen (2016a), Projections of extreme storm surge levels along Europe, *Clim. Dyn.*, *47*, 3171–3190.
- Vousdoukas, M. I., E. Voukouvalas, L. Mentaschi, and L. Feyen (2016b), Developments in large-scale coastal flood hazard mapping, *Nat. Hazards Earth Syst. Sci.*, *16*(8), 1841–1853, doi:10.5194/nhess-16-1841-2016.
- Vousdoukas, M. I., L. Mentaschi, E. Voukouvalas, M. Verlaan, and L. Feyen (2017), Extreme sea levels on the rise along Europe's coasts, *Earth's Futur.*, doi:10.1002/2016EF000505, in press.
- Wang, B., R. Wu, and X. Fu (2000), Pacific-East Asian teleconnection: How does ENSO affect East Asian climate?, *J. Clim.*, *13*(9), 1517–1536, doi:10.1175/1520-0442(2000)013<1517:PEATHD>2.0.CO;2.
- Wang, X. L., V. R. Swail, F. W. Zwiers, X. Zhang, and Y. Feng (2009), Detection of external influence on trends of atmospheric storminess and northern oceans wave heights, *Clim. Dyn.*, *32*(2–3), 189–203, doi:10.1007/s00382-008-0442-2.
- Wang, X. L., Y. Feng, and V. R. Swail (2014), Changes in global ocean wave heights as projected using multimodel CMIP5 simulations, *Geophys. Res. Lett.*, *41*, 1026–1034, doi:10.1002/2013GL058650.
- Yeo, S.-R., and K.-Y. Kim (2015), Decadal changes in the Southern Hemisphere sea surface temperature in association with El Niño–Southern Oscillation and Southern Annular Mode, *Clim. Dyn.*, *45*(11–12), 3227–3242, doi:10.1007/s00382-015-2535-z.
- Young, I. R., S. Zieger, and A. V. Babanin (2011), Global trends in wind speed and wave height, *Science*, *332*(6028), 451–455, doi:10.1126/science.1197219.
- Young, I. R., J. Vinoth, S. Zieger, and A. V. Babanin (2012), Investigation of trends in extreme value wave height and wind speed, *J. Geophys. Res.*, *117*, C00J06, doi:10.1029/2011JC007753.
- Zappa, C. J., M. L. Banner, R. P. Morison, and S. E. Brumer (2016), On the variation of the effective breaking strength in oceanic sea states, *J. Phys. Oceanogr.*, *46*(7), 2049–2061, doi:10.1175/JPO-D-15-0227.1.
- Zheng, F., J. Li, R. T. Clark, and H. C. Nnamchi (2013), Simulation and projection of the Southern Hemisphere annular mode in CMIP5 models, *J. Clim.*, *26*(24), 9860–9879, doi:10.1175/JCLI-D-13-00204.1.
- Zinkina, J., and A. Korotayev (2014), Explosive population growth in Tropical Africa: Crucial omission in development forecasts—Emerging risks and way out, *World Futures*, *70*, 120–139, doi:10.1080/02604027.2014.894868.